IEEE Access
Multidisciplinary ⋮ Rapid Review ⋮ Open Access Journal

Received 19 December 2023, accepted 3 January 2024, date of publication 8 January 2024, date of current version 24 January 2024.

Digital Object Identifier 10.1109/ACCESS.2024.3350733

RESEARCH ARTICLE

A General Study for the Complex Refractive Index Extraction Including Noise Effect Using a Machine Learning-Aided Method

ALIREZA GHORBANI[1], AMIR SAMAN NOOR AMIN[2], AND ALI ABDOLALI[1,2]
[1]Applied Electromagnetic Laboratory, School of Electrical Engineering, Iran University of Science and Technology, Tehran 1684613114, Iran
[2]Department of Electrical Engineering, Iran University of Science and Technology, Tehran 1684613114, Iran

Corresponding author: Amir Saman Noor Amin (a_nooramin@iust.ac.ir)

ABSTRACT This article investigates the extraction of complex refractive indices from the amplitude and phase of the transmitted electric field. In the first step, an incident plane wave has been assumed and the amplitude and phase of the transmitted plane wave is calculated analytically. In this calculation, different values of the complex refractive index have been assumed for the non-magnetic material under test. In fact, the real part and imaginary part of the refractive index are assumed in the range of [1–10] and [0–1], respectively. Furthermore, a general study is made by an assumption of the material thickness to simulation wavelength ratio in the range of [0.01–20]. Due to examining the measurement noise, noisy data are produced for different values of signal-to-noise ratio in the range of [25–40] dB. Due to the difficulties of estimating the refractive index confronted in the theoretical or iterative methods, a Long short-term memory (LSTM) network is proposed and used for the estimation of complex refractive index based on the amplitude and phase of the transmitted electric field. It is shown that the estimation accuracy of about 97% can be achieved in the trained network. Furthermore, the estimation accuracy as a function of thickness-to-wavelength ratio, signal-to-noise ratio, and the values of real and imaginary parts of the refractive index are studied in detail and shown that higher estimation accuracy can be achieved. The simulated results have been confirmed by the measurement for the thickness-to-wavelength ratio below 0.1 and a good agreement has been found. Therefore, the proposed method can replace analytical or repetitive methods as an optimal and more accurate method.

INDEX TERMS Electromagnetics, wave propagation, inverse scattering, parameter characterization, deep learning.

I. INTRODUCTION

Over the past few decades, the need to extract electromagnetic parameters of the materials has grown exponentially due to their wide-ranging applications in medical imaging [1]. To determine this Refractive Index (RI), time-domain spectroscopy can be used on a variety of materials, such as dielectrics [2], semiconductors [3], and superconductors [4]. Evaluating the electromagnetic parameters of the material under test (MUT) heavily relies on analyzing the ratio of the reflected or transmitted waves to the incident wave [5].

The associate editor coordinating the review of this manuscript and approving it for publication was Sandra Costanzo.

The complex RI can be extracted analytically [6], for plane wave excitation although the accuracy is degraded for high loss or high dispersion materials [7]. Furthermore, higher accuracy can be achieved based on iterative algorithms like Newton-Raphson [7] and Nelder-Mead for appropriate initial values [7]. However, the low speed or non-convergence of data analysis limited the applications of these algorithms in real-time processing [7]. If the thickness of the MUT is near or more than the wavelength, the accuracy of the parameters is degraded due to phase ambiguity in both analytical and iterative methods [7].

Recently, the Artificial Neural Network (ANN) has been applied to this application. In [8], the Bayesian regularization

algorithm is used for the extraction of the electromagnetic parameter of the material in the microwave regime. In this calculation, the Debye model has been used for the dispersion and a thin layer of the powder of the material is studied in the coaxial test setup [9]. Similarly, the Levenberg-Marquardt (LM) algorithm is used to train a neural network for the extraction of the complex RI of low-loss thin material in the transmission mode of the THz-TDS setup [10]. For the ANN methods [8], higher accuracy of the parameter extraction is achieved [10], [11].

This research shows that deep learning can be used as an alternative approach to address these issues. By leveraging deep learning methods, we can significantly reduce the complexity and time required to solve the problem while still achieving high precision in the extraction of complex RI. Recurrent neural networks (LSTM) [12], have been used for RI extraction upon plane wave excitation of materials with different thicknesses.

As mentioned earlier, the accuracy of the extraction of the refractive index is mainly affected by the material thickness-to-free space wavelength ratio (d/λ_0) [13]. Typically, as the (d/λ_0) ratio increases, the accuracy of refractive index estimation decreases [14]. To address this issue, it aims to develop a network that can be used for a wide range of (d/λ_0). Another significant issue is the effect of measurement noise on the estimation accuracy. However, real-world measurements often involve noise [15], which an significantly affect parameter estimation accuracy. In this work, the accuracy of estimation of different values of signal-to-noise ratios (SNRs) is studied in detail.

The remainder of this paper is organized as follows. In Sect. ''Data Preparation'' The analytical background of the study is studied and the classification of data in the matrix form will be discussed. Then, in Sect. ''Implementation of LTSM Neuronal Network'', the deep learning method for the implementation of the proposed neural network is examined. The performance analysis and estimation accuracy of the proposed network based on the simulation and measurement results are studied in the ''Performance Analysis and Discussion'' section. Finally, some conclusions are remarked.

II. DATA PREPARATION

The flow chart of the proposed method is shown in FIGURE 1. In the first step, the transmitted electric field is calculated analytically for different values of the complex refractive index and thickness-to-wavelength ratio. Furthermore, noisy data are also produced for the incorporation of measurement noise. Then, the prepared data are classified and matrices are formed for training the proposed deep learning network (FIGURE 1.a). After that, a Long short-term memory (LSTM) is formed, and trained, and the accuracy is validated (FIGURE 1.b). Finally, the performance of the proposed network is analyzed in detail as a function of complex refractive index, thickness-to-wavelength ratio, and signal-to-noise ratio. based on the above-mentioned procedure, the rest of the article is dedicated to the detailed study of each issue.

III. THEORETICAL BACKGROUND

In this research, the extraction of complex refractive indices has been done by the study of traveling waves through the material [16]. For this purpose, the temporal profile of the pulse that travels through the material is obtained by convolving the radiated waveform with the impulse response of the material in the time domain [17]. The impulse response of the MUT can be obtained by comparing two electric fields in the frequency domain: the incident electric field $E_{inc}(\omega)$ and the transmitted electric field, signal $E_{tx}(\omega)$. Therefore, we have

$$\tilde{H}_{MUT}(\omega) = \frac{E_{tx}(\omega)}{E_{inC}(\omega)} \tag{1}$$

$$\tilde{H}_{MUT}(\omega) = \frac{4\tilde{n}(\omega)}{(\tilde{n}(\omega)+1)^2} e^{-i\tilde{n}(\omega)2\pi(d/\lambda)/c} = Ae^{i\varphi_{MUT}} \tag{2}$$

$$\varphi_{MUT}(\omega) = (n(\omega)-1)\frac{2\pi}{d/\lambda} \tag{3}$$

$$\tilde{n}(\omega) = n + ik \tag{4}$$

$\tilde{H}_{MUT}$ and φ_{MUT} stand for the complex frequency response and its phase for MUT. Furthermore, $\tilde{n}(\omega)$, d, and λ represent the complex refractive index, the MUT thickness, the free space wavelength, and the complex propagation constant. The real part and imaginary part of the refractive index are denoted by n and k, respectively. Due to two unknown parameters n and k, consistent results can be obtained by solving equation (2). Therefore, a deep learning network is utilized to determine the values of n and k from $\tilde{H}_{MUT}(\omega)$ and will show that highly accurate results can be obtained.

IV. MATRIX FORMATION

As mentioned earlier, the process of generating simulated training sets involves creating an input pulse using a function in MATLAB that produces a shape similar to that of an experimentally measured pulse. This pulse is then propagated through a material with given parameters for refractive index, thickness, and transmission coefficients. The values of n, k, and frequency are varied to generate a range of simulated samples, which are used to train a neural network using a supervised learning approach. The neural network accepts an input array of floating point numbers and produces an output array based on the input. The length of the dataset is expected to affect the prediction loss of the model. It is important to note that while the given data describes the basic process for generating simulated training sets and training a neural network using supervised learning, there may be additional steps or considerations depending on the specific application and goals of the projects.

In this research, 20,000 data points within a specified range of parameters have been generated, as follows,

$$n \in [0, 10] \tag{5}$$

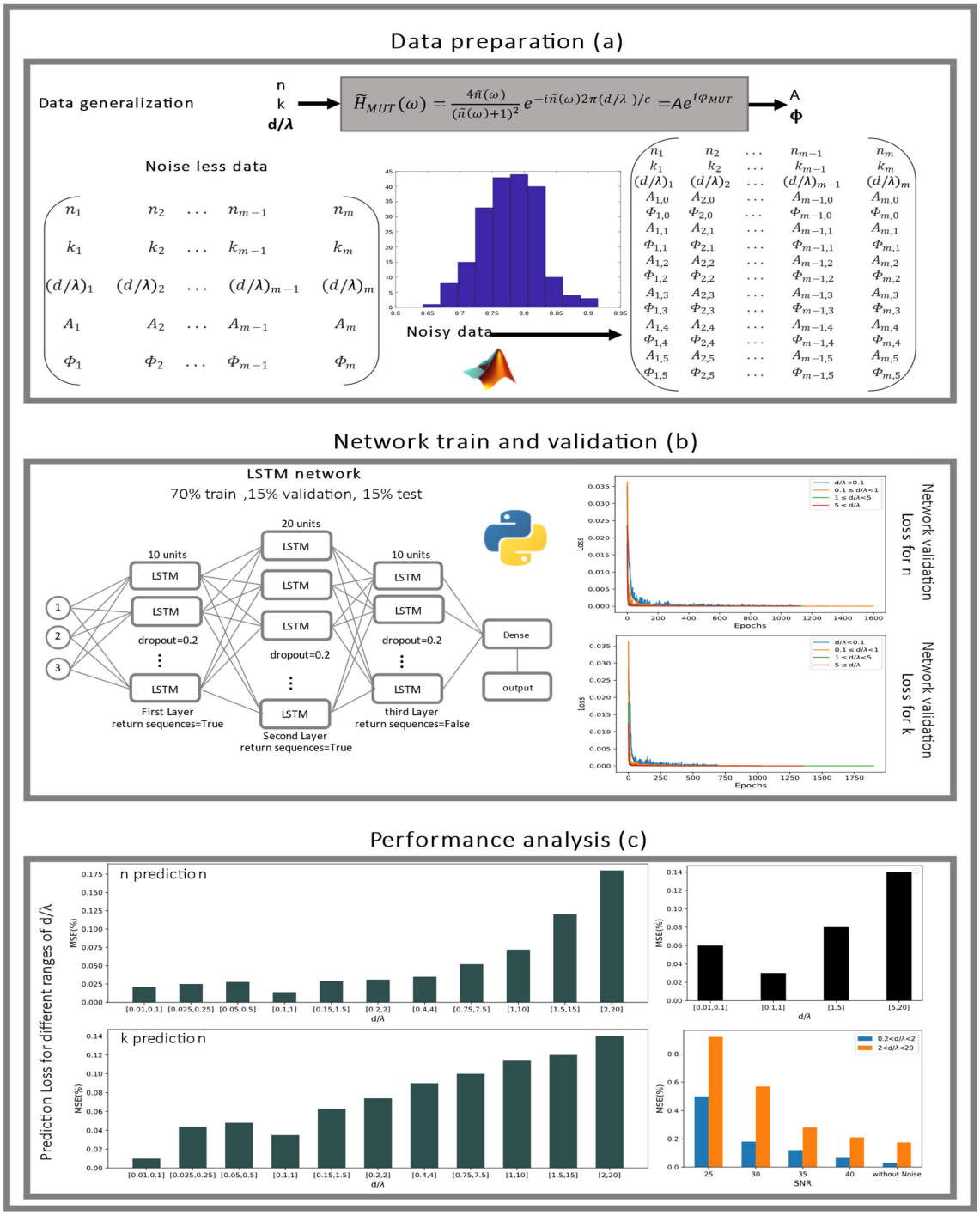

FIGURE 1. Flow chart of the proposed algorithm for the estimation of complex refractive index.

$$k \in [0, 1] \tag{6}$$

$$d/\lambda \in \left[\frac{1}{100}, 20\right] \tag{7}$$

In noiseless simulations, the following matrix representations have been used. The dimension index of the vectors is denoted by m, in which $m = 20000$. It is worth mentioning that a uniform random generator is utilized for the generation of data in the above-mentioned ranges. The generated vectors and the matrix representation are as follows,

$$d/\lambda = [(d/\lambda)_1, (d/\lambda)_2, (d/\lambda)_2, \ldots, (d/\lambda)_{m-2}, (d/\lambda)_{m-1},]$$
$$(d/\lambda)_m \qquad \text{Thickness/wavelength} \tag{8}$$

$$A = [A_1, A_2, A_3, A_4, \ldots, A_{m-2}, A_{m-1}, A_m]$$
$$\text{Amplitude} \tag{9}$$

$$\Phi = [\Phi_1, \Phi_2, \Phi_3, \Phi_4, \ldots, \Phi_{m-2}, \Phi_{m-1}, \Phi_m]$$
$$\text{Phase} \tag{10}$$

$$n = [n_1, n_2, n_3, n_4, \ldots, n_{m-2}, n_{m-1}, n_m]$$
Real part of refractive index (11)

$$k = [k_1, k_2, k_3, k_4, \ldots, k_{m-2}, k_{m-1}, k_m]$$
Imaginary part of refractive (12)

The generated data matrix which is used for training the deep neural network is:

$$\begin{bmatrix} n_1 & n_2 & \cdots & n_{m-1} & n_m \\ k_1 & k_2 & \cdots & k_{m-1} & k_m \\ (d/\lambda)_1 & (d/\lambda)_2 & \cdots & (d/\lambda)_{m-1} & (d/\lambda)_m \\ A_1 & A_2 & \cdots & A_{m-1} & A_m \\ \Phi_1 & \Phi_2 & \cdots & \Phi_{m-1} & \Phi_m \end{bmatrix}$$

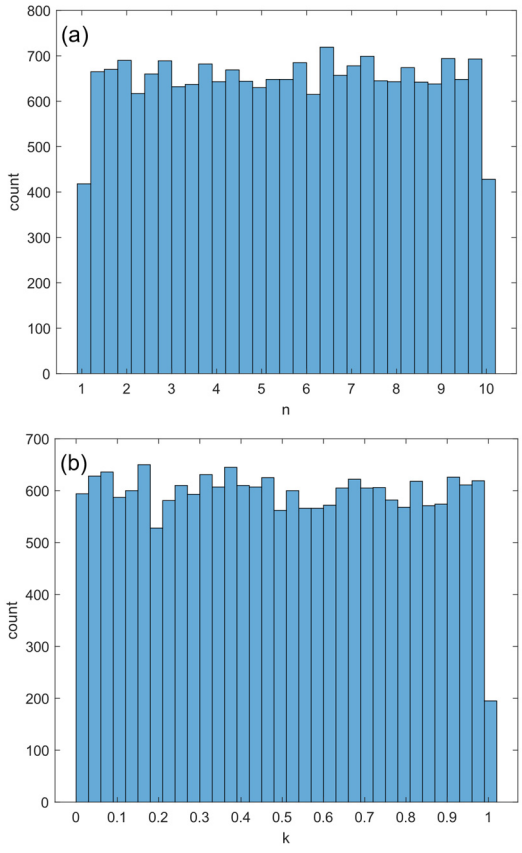

FIGURE 2. Noiseless data distribution of (a) n and (b) k.

In FIGURE 2.a and FIGURE 2.b the histogram of the generated data has been plotted. As shown in this figure, the values on n and k are approximately distributed uniformly in the range of [1,10] and [0,1], respectively. Furthermore, the mentioned distributions are shown for different ranges, as shown in FIGURE 3.a and FIGURE 3.b. This is shown clearly that an approximately uniform distribution has been achieved in each range of $^{d}/_{\lambda}$.

In the noisy scenario, a white Gaussian noise generator is used for the production of noisy data, because the noise generated in a spectrum analyzer can be modeled as Gaussian noise [18]. For each noiseless data, l = 5 noisy data are

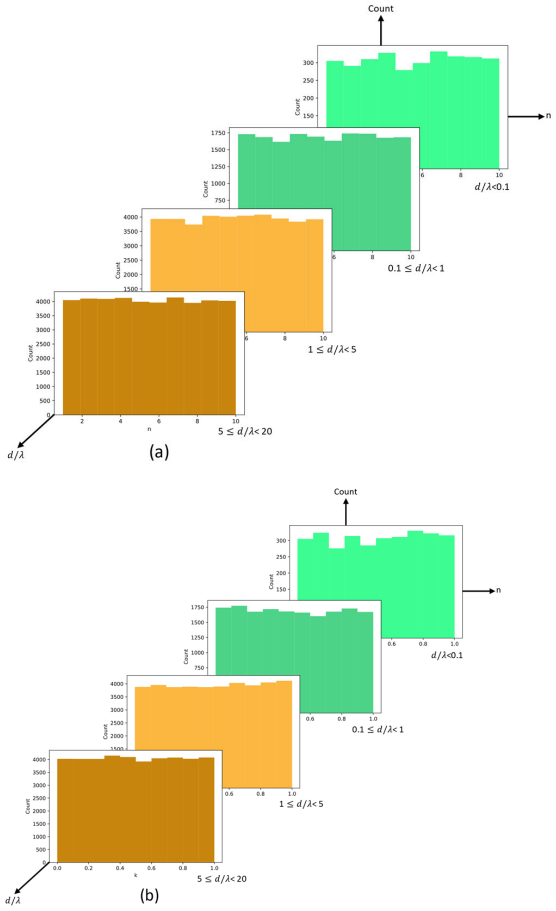

FIGURE 3. Noisy data distribution for different ranges of d/λ for (a) n and (b) k.

generated that fulfill the following conditions:

$$SNR = \frac{P_{signal}}{P_{noise}} = \left(\frac{A_{signal}}{A_{noise}}\right)^2 \quad (13)$$

$$SNR(\text{dB}) = 10log\left(\frac{P_{signal}}{P_{noise}}\right) = 20log\left(\frac{A_{signal}}{A_{noise}}\right) \quad (14)$$

Here, the values of SNR = 25, 30, 35, and 40 are assumed. The amplitude and phase distribution of the prepared data for l=100 are plotted in FIGURE 4.a and FIGURE 4.b, respectively. The noisy data has been generated by a Gaussian random generator in which the standard deviation relatives to SNRs [19]. As can be seen in this figure, a Gaussian distribution is formed as expected.

For the noisy data: m index is the number of data, $m = (l + 1) \times 2{\times}10^4$, (15)–(19), as shown at the bottom of the next page

The generated noisy data matrix which is used for training, as shown in the equation at the bottom of the next page.

V. IMPLEMENTATION OF LTSM NEURAL NETWORK

The main goal of this research is the development of a neural network for the estimation of the values of n and k based on the transmitted electric field.

To achieve this goal, a deep learning model is trained in which the amplitude and phase of transmission coefficient in addition to d/λ are assumed as the inputs, and n and k are regarded as the output features. Once the network is trained, the output features can be estimated based on the input parameters.

In this research, an LSTM (Long Short-Term Memory) network is proposed for this purpose. this type of network is a recurrent neural network that can retain information over long periods. LSTMs are well-suited for training, predicting, and classifying different types of data [12].

To ensure that the deep learning network generalizes well to unseen data, techniques such as cross-validation, regularization, and data augmentation have been implemented during training and continuously monitor the model's performance [20].

In this research, the proposed LSTM network consists of three LSTM layers, a Dense layer, and a Sigmoid activation function. The prepared data are divided into three categories: training data (70%), validation data (15%), and testing sets (15%). Furthermore, the number of epochs is limited to 3000. Here, the dropout layers within the network are implemented to avoid overfitting. The implementation of the model has been done using Python version 3.7.13 and the TensorFlow 2 Deep Learning framework.

If The output of the neural network includes a two-order vector including the real part of the refractive index and the imaginary part of the refractive index. In our network activation function is sigmoid, and optimizer is rmsprop, batch size is 64 drop out is 0.2 and the maximum number of epochs is 3000. The utility cost function MSE has been used to calculate the difference between the real value and the estimated value [21].

$$MSE = \frac{1}{N}\sum_{i-1}^{m}(f_i - y_i)^2 \tag{20}$$

VI. PERFORMANCE ANALYSIS AND DISCUSSION

The loss diagrams of the proposed model for n and k are shown in FIGURE 6.a and FIGURE 6.b. As shown in this figures, the values of MSE are achieved at 0.03%, and 0.03% for real and imaginary parts of the refractive index in the [0.1, 1] range for d/λ, respectively. Furthermore, the identity of validation loss to training loss reveals avoidance of overfitting in the proposed network. The training procedure and the estimation of one sample of complex refractive index take 8280 and <1 seconds using a system equipped with an Intel Core i7-10700K processor and 16GB RAM.

The evaluation method of the proposed network can be studied in four categories. In the first category, the complex

$$d/\lambda = \begin{bmatrix} \left[\left(\frac{d}{\lambda}\right)_1, \left(\frac{d}{\lambda}\right)_1, \ldots, \left(\frac{d}{\lambda}\right)_1\right]_{1\times(l+1)}, \\ \left[\left(\frac{d}{\lambda}\right)_2, \left(\frac{d}{\lambda}\right)_2, \ldots, \left(\frac{d}{\lambda}\right)_2\right]_{1\times(l+1)}, \ldots, \\ \left[\left(\frac{d}{\lambda}\right)_m, \left(\frac{d}{\lambda}\right)_m, \left(\frac{d}{\lambda}\right)_m\right] 1 \times (l+1) \end{bmatrix} \tag{15}$$

$$A = \begin{bmatrix} [A_{11}, A_{12}, \ldots, A_{1l}]_{1\times(l+1)}, [A_{21}, A_{22}, \ldots, A_{2l}]_{1\times(l+1)}, \ldots, \\ [A_{m1}, A_{m2}, \ldots, A_{ml}]_{1\times(l+1)} \end{bmatrix} \tag{16}$$

$$\Phi = \begin{bmatrix} [\Phi_{11}, \Phi_{12}, \ldots, \Phi_{1l}]_{1\times(l+1)}, [\Phi_{21}, \Phi_{22}, \ldots, \Phi_{2l}]_{1\times(l+1)}, \ldots, \\ [\Phi_{m1}, \Phi_{m2}, \ldots, \Phi_{ml}]_{1\times(l+1)} \end{bmatrix} \tag{17}$$

$$n = \begin{bmatrix} [n_1, n_1, \ldots, n_1]_{1\times(l+1)}, [n_2, n_2, \ldots, n_2]_{1\times(l+1)}, \ldots, \\ [n_m, n_m, n_m]_{1\times(l+1)} \end{bmatrix} \tag{18}$$

$$k = \begin{bmatrix} [k_1, k_1, \ldots, k_1]_{1\times(l+1)}, [k_2, k_2, \ldots, k_2]_{1\times(l+1)}, \ldots, \\ [k_m, k_m, k_m]_{1\times(l+1)} \end{bmatrix} \tag{19}$$

$$\begin{bmatrix} n_1 & n_2 & \cdots & n_{m-1} & n_m \\ k_1 & k_2 & \cdots & k_{m-1} & k_m \\ (d/\lambda)_1 & (d/\lambda)_2 & \cdots & (d/\lambda)_{m-1} & (d/\lambda)_m \\ A_{1,0} & A_{2,0} & \cdots & A_{m-1,0} & A_{m,0} \\ \Phi_{1,0} & \Phi_{2,0} & \cdots & \Phi_{m-1,0} & \Phi_{m,0} \\ A_{1,1} & A_{2,1} & \cdots & A_{m-1,1} & A_{m,1} \\ \Phi_{1,1} & \Phi_{2,1} & \cdots & \Phi_{m-1,1} & \Phi_{m,1} \\ A_{1,2} & A_{2,2} & \cdots & A_{m-1,2} & A_{m,2} \\ \Phi_{1,2} & \Phi_{2,2} & \cdots & \Phi_{m-1,2} & \Phi_{m,2} \\ A_{1,3} & A_{2,3} & \cdots & A_{m-1,3} & A_{m,3} \\ \Phi_{1,3} & \Phi_{2,3} & \cdots & \Phi_{m-1,3} & \Phi_{m,3} \\ A_{1,4} & A_{2,4} & \cdots & A_{m-1,4} & A_{m,4} \\ \Phi_{1,4} & \Phi_{2,4} & \cdots & \Phi_{m-1,4} & \Phi_{m,4} \\ A_{1,5} & A_{2,5} & \cdots & A_{m-1,5} & A_{m,5} \\ \Phi_{1,5} & \Phi_{2,5} & \cdots & \Phi_{m-1,5} & \Phi_{m,5} \end{bmatrix}$$

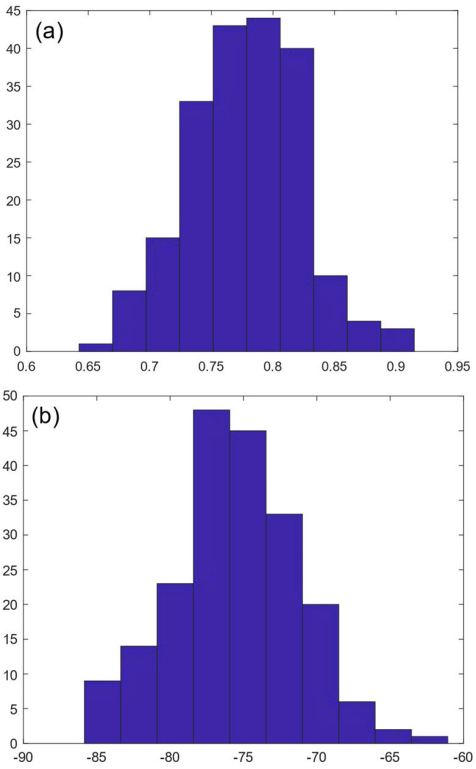

FIGURE 4. The distribution of (a) amplitude and (b) phase for (S/N)=40 dB.

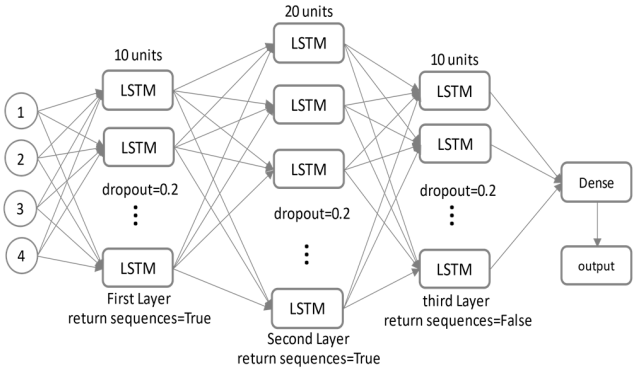

FIGURE 5. Used LSTM network architecture.

refractive index has been estimated for different values of d/λ as explained in A. In the second category, the statistical analysis of the network loss in the estimation of the refractive index has been done for different values of d/λ as studied in B. Considering the noise effect on statistical network loss is the issue of the second category and analyzed in C. Finally, the proposed network has been used for the estimation of the complex refractive index based on the measurement results, as discussed in D.

A. NETWORK EVALUATION IN REFRACTIVE INDEX ESTIMATION

In the first step, the evaluation of the proposed method has been done by comparing the estimated and accurate values of the complex refractive index of MUT. In this comparison,

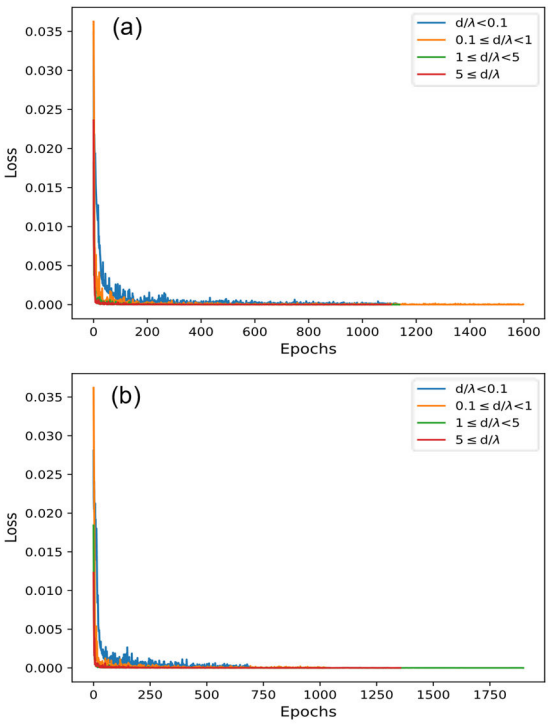

FIGURE 6. Used LSTM network architecture. Training validation loss progress as a function of Epochs for (a) the real part and (b) the imaginary part of the refractive index.

different values of d/λ and complex refractive index have been considered as represented in TABLE 1. In this table, it is clearly shown that the relative error in the estimation of the complex refractive index is less than – for $0.04 < d/\lambda < 12$. Here, the values of $0 < n < 10$ and $k < 1$ are considered.

B. STATISTICAL EVALUATION OF THE NETWORK IN THE ESTIMATION OF COMPLEX REFRACTIVE INDEX

In this subsection, the performance of the proposed network has been studied statistically in the estimation of complex refractive index. For this purpose, the MSE parameter has been considered for different ranges of d/λ, as shown in FIGURE 7. In this figure, four ranges of [0.01,0.1], [0.1,1], [1,5], and [5,20] are considered for d/λ. based on the presented results in FIGURE 7, it can be concluded that an estimation accuracy is slightly degraded for higher values of d/λ. This conclusion follows analytical results, although more precise results are achieved in the proposed method [22].

More precise statistical analysis has been done by considering the same length for d/λ ranges, as shown in FIGURE 8. In this figure, the $0.01 < d/\lambda < 20$ range is divided into 11 one-decade wavelength ranges. It is expected that these ranges to overlap. Considering one-decade wavelength ranges, higher MSE in the estimation of n and k belongs to higher values of d/λ, as depicted in FIGURE 8.a and Figure 8.b, respectively. This conclusion follows the previous one and analytical methods [22].

TABLE 1. The estimated complex refractive index for different values of d/Λ.

Sample Thickness	value	accurate	estimate d	Relative error(%)
d/λ= 0.043	n	8.263	8.2741	0.0123
	k	0.0673	0.0684	1.21E-04
d/λ= 0.079	n	1.138	1.1305	5.62E-03
	k	0.963	0.9519	0.0123
d/λ= 1.992	n	4.29	4.3201	0.0906
	k	0.115	0.0958	0.0369
d/λ= 2.524	n	6.829	6.8521	0.0534
	k	0.967	0.9408	0.0686
d/λ= 0.138	n	3.245	3.2301	0.0222
	k	0.654	0.6684	0.0207
d/λ= 0.981	n	8.22	8.2047	0.0234
	k	0.252	0.2419	0.0102
d/λ= 5.408	n	9.263	9.2301	0.1082
	k	0.639	0.6684	0.0864
d/λ=11.744	n	1.638	1.5948	0.1866
	k	0.561	0.5916	0.0936

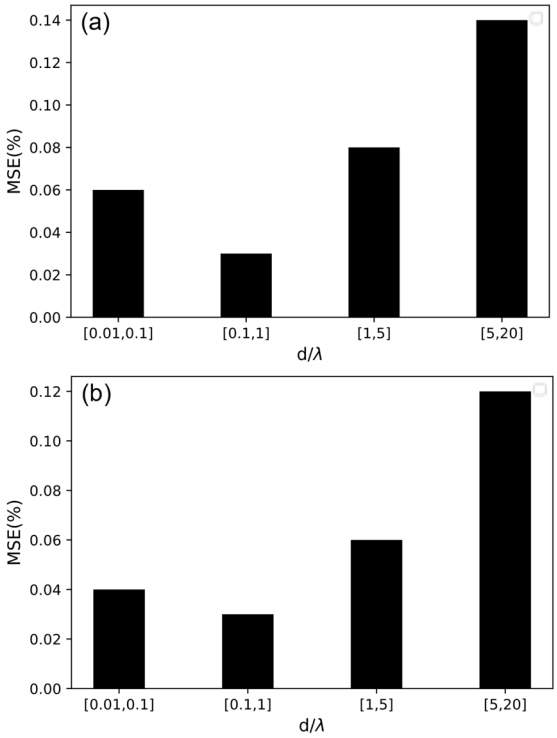

FIGURE 7. MSE for different ranges of d/λ for (a) n estimation results and (b) k prediction results.

The analysis of MSE for the prediction of n and k as a function of wavelength range is shown in Figure 9.a and Figure 9.b, respectively. In this figure, it is clearly shown that the accuracy of the prediction remains relatively constant from one-octave to one-decade ranges. This conclusion indicates the appropriate performance of the proposed network, which can perform an estimation with minimized error almost independently of the interval length.

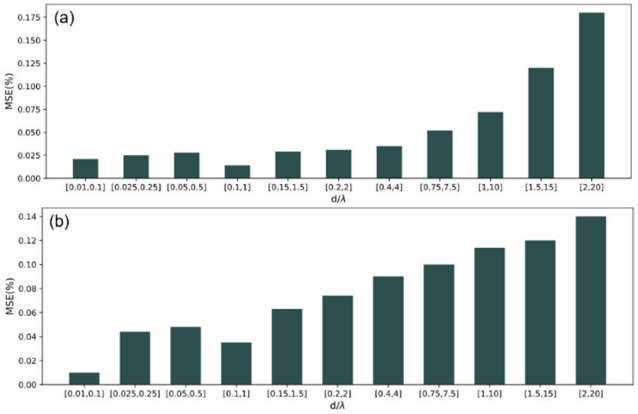

FIGURE 8. Prediction Loss for different ranges of d/λ(a) n prediction results and (b) k prediction result.

To analyze the error estimation as a function of the refractive index values, a one-decade range of $0.1<d/\lambda<1$ has been considered. Then, the trained network is used for the estimation of 1000 complex refractive index values. Afterward, the MSEs in the estimation of n and k have been calculated and plotted in FIGURE 10.a and FIGURE 10.b, respectively. Due to the presented data in this figure, it can be concluded that lower values of n or k can be estimated more accurately.

C. STATISTICAL EVALUATION OF THE NETWORK IN THE ESTIMATION OF COMPLEX REFRACTIVE INDEX CONSIDERING NOISE EFFECT

After evaluating the performance of the proposed network with noise-free data, we will further investigate the effect of noise on the estimation error. For this, data are generated for four values of SNRs as explained earlier, and are used for training the proposed network. Then, this network has been used for the estimation of 1000 values of complex refractive indices in two one-decade ranges $0.1<d/\lambda<2$ and $2<d/\lambda<20$. Afterward, the MSEs of prediction are calculated and plotted, as shown in FIGURE 11. Here, the MSE of estimation of n and k are plotted in FIGURE 11.a and FIGURE 11.b. Considering the presented results in this figure, three aspects can be highlighted. First, The estimation error decreases with an almost linear slope as a function of the signal-to-noise ratio in the logarithmic scale. Second, the estimation error remains constant for SNR=40dB and noiseless data. This fact determines the necessary value of the signal-to-noise ratio to operate the system with minimum error. Third, similar to the noiseless network, the estimation accuracy degraded for higher values of d/λ by considering noise.

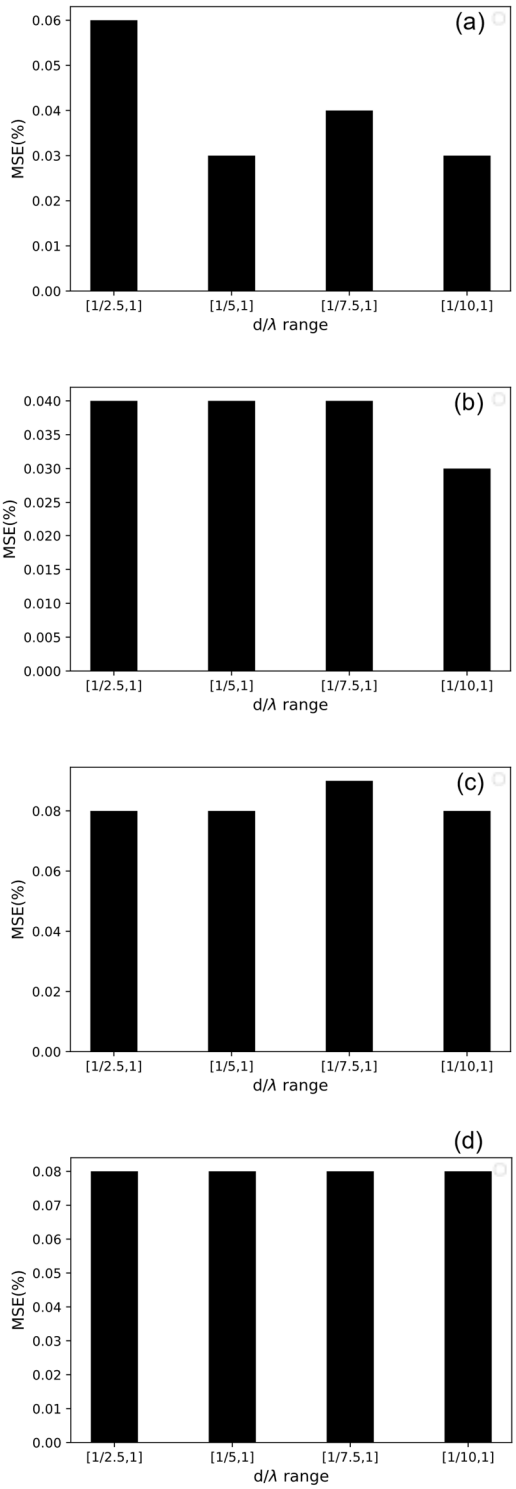

FIGURE 9. The analysis of MSE as a function of the wavelength range. (a) MSE of n prediction for d/λ in [0.2,2] and (b) MSE of k prediction for d/λ in [0.2,2], (c) MSE of n prediction for d/λ in [2, 20] and (d) MSE of k prediction for d/λ in [2, 20].

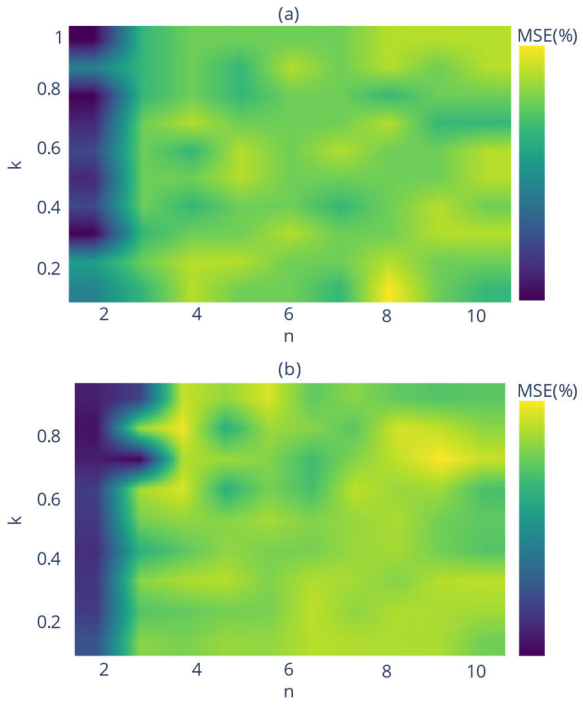

FIGURE 10. The distribution of MSE for the estimation of (a) n and (b) k.

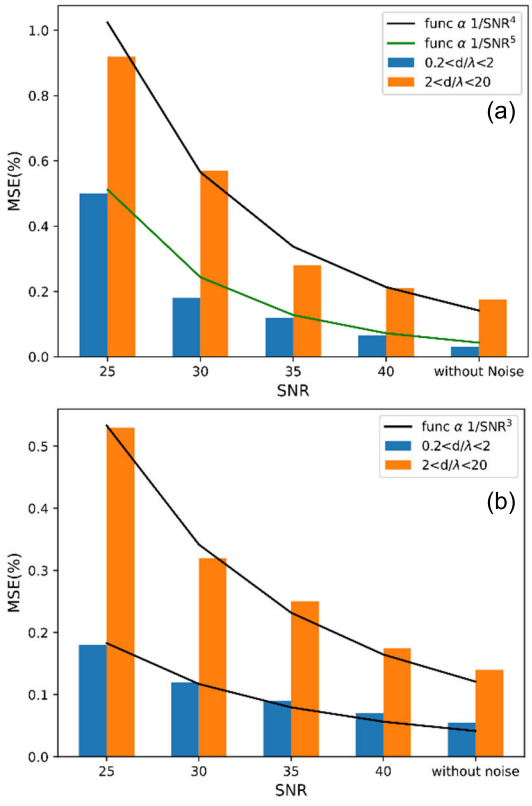

FIGURE 11. Prediction Loss for different ranges of d/λ with considering noise, MSE for prediction of (a) n and (b) k.

D. MEASUREMENTS

After evaluating the performance of the proposed network with noise-free and noisy data, we further assessed our method using measurement results. We utilized two double-ridged horn antennas manufactured in our antenna laboratory.

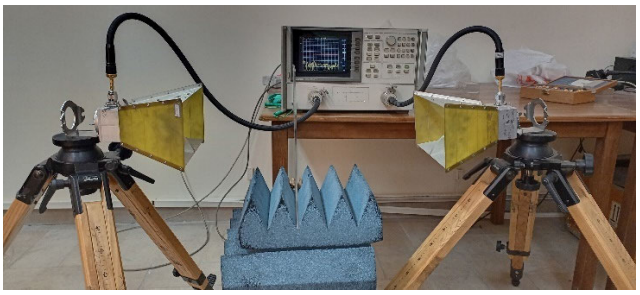

FIGURE 12. Experimental measurement setup.

TABLE 2. The estimated complex refractive index for different values of d/Λ.

Sample Frequency	value	accurate	measured
2.6 GHz	n	1.49	1.4845
	k	0.02	0.0208
2 GHz	n	1.49	1.4961
	k	0.02	0.0209
1.5 GHz	n	1.49	1.4801
	k	0.02	0.0190
1 GHz	n	1.49	1.5036
	k	0.02	0.0218

Additionally, we employed a VNA (8720D Microwave Vector Network Analyzer). As shown in FIGURE 12, a Plexiglas sheet is positioned between two antennas to measure the phase and amplitude of the transmitted field. The thickness of sheet is 4 mm.

The distance between the two antennas is 65 cm. In our case, the far-field range of the antennas are about 32 cm at the 2.6 GHz. Therefore, the assumption of plane wave radiation is valid for the frequency range of [1- 2.6] GHz and the complex transmitted wave (S_{21}) is measured with and without the Plexiglas sheet. After the calibration process, these data are used for the estimation of the complex refractive index for the sample range of $0.01 < \frac{d}{\lambda} < 0.1$, as depicted in TABLE 2. In this table, the values of the complex refractive index are estimated at the frequencies of 1GHz, 1.5GHz, 2GHz, and 2.6GHz and are in good agreement with accurate ones.

VII. CONCLUSION

In this paper, the extraction of complex refractive index has been considered for non-magnetic materials. Due to the limitation of theoretical or iterative methods, an LSTM neural network has been proposed for this purpose. The phase and amplitude of the transmitted plane wave are assumed as the inputs while the real and imaginary parts of the complex refractive index of MUT are considered as the outputs. The proposed network has been trained for values of $1<n<10$, $0<k<1$, and $0.01<d/\lambda<20$ and used for estimation of n and k. It is shown that the complex refractive index can be estimated with an error of less than 0.1% while the estimation accuracy arises by decreasing the material thickness-to-free space wavelength ratio of MUT. Furthermore, the analysis shows that the estimation accuracy remains relatively constant for different ranges of material thickness to free space wavelength from one decade to one octave. Furthermore, the estimation accuracy degraded for higher values of real or imaginary parts of the refractive index. Finally, the performance of the system was evaluated for noisy data, which is an important issue in measurement setups. Considering Signal to noise ratio in the range of [25-40] dB for inputs, it is shown that the prediction error decreases linearly as a function of SNR. Furthermore, the same prediction error is achieved on the assumption of SNR=40 dB and a noiseless network. Therefore, the required signal-to-ratio to achieve the best performance of the network can be determined.

REFERENCES

[1] Q. Wang, L. Xie, and Y. Ying, "Overview of imaging methods based on terahertz time-domain spectroscopy," *Appl. Spectrosc. Rev.*, vol. 57, no. 3, pp. 249–264, Mar. 2022.

[2] D. Grischkowsky, S. Keiding, M. van Exter, and C. Fattinger, "Far-infrared time-domain spectroscopy with terahertz beams of dielectrics and semiconductors," *J. Opt. Soc. Amer. B, Opt. Phys.*, vol. 7, no. 10, p. 2006, Oct. 1990.

[3] M. van Exter and D. Grischkowsky, "Optical and electronic properties of doped silicon from 0.1 to 2 THz," *Appl. Phys. Lett.*, vol. 56, no. 17, pp. 1694–1696, Apr. 1990.

[4] J. F. Whitaker, F. Gao, and Y. Liu, "Terahertz-bandwidth pulses for coherent time-domain spectroscopy," *SPIE*, vol. 2145, pp. 168–177, Feb. 1994.

[5] J. G. D. Oliveira, J. G. D. Junior, E. N. M. G. Pinto, V. P. S. Neto, and A. G. D'Assunção, "A new planar microwave sensor for building materials complex permittivity characterization," *Sensors*, vol. 20, no. 21, p. 6328, Nov. 2020.

[6] H. Gu, S. Zhu, B. Song, M. Fang, Z. Guo, X. Chen, C. Zhang, H. Jiang, and S. Liu, "An analytical method to determine the complex refractive index of an ultra-thin film by ellipsometry," *Appl. Surf. Sci.*, vol. 507, Mar. 2020, Art. no. 145091.

[7] N. Klokkou, J. Gorecki, J. S. Wilkinson, and V. Apostolopoulos, "Artificial neural networks for material parameter extraction in terahertz time-domain spectroscopy," *Opt. Exp.*, vol. 30, no. 9, p. 15583, Apr. 2022.

[8] T. Mosavirik, M. Hashemi, M. Soleimani, V. Nayyeri, and O. M. Ramahi, "Accuracy-improved and low-cost material characterization using power measurement and artificial neural network," *IEEE Trans. Instrum. Meas.*, vol. 70, pp. 1–9, 2021.

[9] T. Mosavirik, M. Hashemi, M. Soleimani, V. Nayyeri, and O. M. Ramahi, "Material characterization using power measurements: Miracle of machine learning," in *Proc. 51st Eur. Microw. Conf. (EuMC)*, Apr. 2022, pp. 606–609.

[10] T. Mosavirik, V. Nayyeri, M. Hashemi, M. Soleimani, and O. M. Ramahi, "Direct permittivity reconstruction from power measurements using a machine learning aided method," *IEEE Trans. Microw. Theory Techn.*, 2023.

[11] T. Mosavirik, M. Soleimani, V. Nayyeri, S. H. Mirjahanmardi, and O. M. Ramahi, "Permittivity characterization of dispersive materials using power measurements," *IEEE Trans. Instrum. Meas.*, vol. 70, pp. 1–8, 2021.

[12] Y. Yu, X. Si, C. Hu, and J. Zhang, "A review of recurrent neural networks: LSTM cells and network architectures," *Neural Comput.*, vol. 31, no. 7, pp. 1235–1270, Jul. 2019.

[13] G. Georgescu and A. Petris, "Analysis of thickness influence on refractive index and absorption coefficient of zinc selenide thin films," *Opt. Exp.*, vol. 27, no. 24, p. 34803, Nov. 2019.

[14] C. W. O'Dell, D. S. Swetz, and P. T. Timbie, "Calibration of millimeter-wave polarimeters using a thin dielectric sheet," *IEEE Trans. Microw. Theory Techn.*, vol. 50, no. 9, pp. 2135–2141, Sep. 2002.

[15] R. Tauk, F. Teppe, S. Boubanga, D. Coquillat, W. Knap, Y. M. Meziani, C. Gallon, F. Boeuf, T. Skotnicki, C. Fenouillet-Beranger, D. K. Maude, S. Rumyantsev, and M. S. Shur, "Plasma wave detection of terahertz radiation by silicon field effects transistors: Responsivity and noise equivalent power," *Appl. Phys. Lett.*, vol. 89, no. 25, pp. 1–12, Dec. 2006.
[16] Y. Makhlouka, F. Sanaâ, and M. Gharbia, "Ordinary and extraordinary complex refractive indices extraction of a mylar film by transmission spectrophotometry," *Polymers*, vol. 14, no. 9, p. 1805, Apr. 2022.
[17] Y. Liu, S.-G. Park, and A. M. Weiner, "Terahertz waveform synthesis via optical pulse shaping," *IEEE J. Sel. Topics Quantum Electron.*, vol. 2, no. 3, pp. 709–719, Mar. 1996.
[18] F. Gustrau, *RF and Microwave Engineering: Fundamentals of Wireless Communications*. Hoboken, NJ, USA: Wiley, 2012.
[19] A. Yildirim and S. Kiranyaz, "1D convolutional neural networks versus automatic classifiers for known LPI radar signals under white Gaussian noise," *IEEE Access*, vol. 8, pp. 180534–180543, 2020.
[20] L. Zhang, J. Tan, D. Han, and H. Zhu, "From machine learning to deep learning: Progress in machine intelligence for rational drug discovery," *Drug Discovery Today*, vol. 22, no. 11, pp. 1680–1685, Nov. 2017.
[21] O. Köksoy, "Multiresponse robust design: Mean square error (MSE) criterion," *Appl. Math. Comput.*, vol. 175, no. 2, pp. 1716–1729, Apr. 2006.
[22] T. D. Dorney, R. G. Baraniuk, and D. M. Mittleman, "Material parameter estimation with terahertz time-domain spectroscopy," *J. Opt. Soc. Amer. A, Opt. Image Sci.*, vol. 18, no. 7, p. 1562, Jul. 2001.

ALIREZA GHORBANI received the B.Sc. degree in electrical engineering from the Azarbaijan Shahid Madani University of Tabriz (ASMU), Tabriz, Iran, in 2020. He is currently pursuing the M.Sc. degree in electrical engineering with the Iran University of Science and Technology (IUST).

His current research interests include electromagnetics, scattering, optics, quantum, and nanoparticles.

AMIR SAMAN NOOR AMIN received the B.Sc., M.Sc., and Ph.D. degrees in electrical engineering from the University of Tehran, Tehran, Iran, in 2007, 2009, and 2016.

He is currently an Associate Professor with the School of Electrical Engineering, Iran University of Science and Technology (IUST), Tehran. His current research interests include scattering, optics, microwave sensors and measurements, and time-domain spectroscopy.

ALI ABDOLALI was born in Tehran, Iran, in 1974. He received the B.Sc. degree in electrical engineering from the University of Tehran, Tehran, in 1998, the M.Sc. degree in electrical engineering from Tarbiat Modares University, Tehran, in 2000, and the Ph.D. degree in electrical engineering from the Iran University of Science and Technology (IUST), Tehran, in 2010. He joined the Department of Electrical Engineering, IUST, where he is currently a Full Professor of electromagnetic engineering. He has authored or coauthored more than 241 papers in international journals and conferences. His current research interests include electromagnetic wave scattering, radar cross section and RCSR, radar absorbing materials, cloaking, metamaterials, and wave propagation in complex media (anisotropic, inhomogeneous, and dispersive media), frequency-selective surfaces, and bioelectromagnetic.